Progress In Electromagnetics Research M, Vol. 109, 179–189, 2022

Poly-Resonator Lowpass Filter for 26th Order Harmonic Suppression

Thevaruparambil A. Nisamol[1, *], Parambil Abdulla[1], and Thulaseedharan K. Rekha[2]

Abstract—In this brief, an ultra-vast stopband lowpass filter with miniaturized circuit size for 26th harmonic suppression using poly-resonators and an inclined stepped-impedance transmission line (ISTL) is developed. The poly-resonators such as radial stub resonator and resonator modules constitute the significant part of the filter, and the discontinuity in the inclined angle of the ISTL is balanced by 75% chamfering. The coupling with ISTL has influence over the stopband behavior, and the equivalent circuit for the first transmission zero is analysed. The normalised circuit size is reduced to 16.6%, and additional frequency rejection is achieved using resonator modules RM_1 and RM_2. The relative stopband width of 185.4% is attained with a 3 dB cut-off frequency of 1.51 GHz. L band communication applications having circuit area limitations can make use of the Poly-resonator ISTL filter for achieving high-frequency noise rejection.

1. INTRODUCTION

The wide range applications of L band filter circuits in the field of satellite navigation, iridium telecommunication satellite phones, aircraft surveillance, amateur radio, digital audio/video/multimedia broadcasting, etc. obligate the frequency performance parameters which is highly pivotal. Since the other band circuits occupy the same platform, high-frequency interferences outside the transition frequency must be eliminated throughout a wide range of harmonics. The filter structures can be employed as a harmonics controller in the envelope detector and can be integrated prior to other circuits [1]. However, due to space restrictions, the highest achievable relative stopband (RSB) is limited. [2–6] displays a number of lowpass filter geometries, some of which are used in conjunction with other active circuits [7–10]. The bandpass filter spectrum applied in WiMAX [7] and power divider requirements [10] have been put to use the compact lowpass filter circuits working in the same band. Modifying the low impedance patch side of the resonators improves the roll-off characteristics [11], but the attenuation performance in those systems is often inadequate. Wide tuning can be achieved with pin diodes [12] or tunable capacitors, depending on the cut-off frequency need. The key inherent properties of filters, such as normalized circuit size (NCS) and RSB, might affect this in general. The NCS must be kept within the constraints, which is normally accomplished by altering the resonators and reducing the visible size. This will have a negative impact on the application's cut-off criteria. Use of complimentary split ring resonators [13], a sort of defective ground structure, is another way to reduce the filter's size. Although the cut-off frequency slope has improved marginally, the stopband rejection has remained poor, necessitating the usage of more circuit area. To make the filter circuit even smaller, a spur line approach [14] with a defective ground structure is applied. Although the circuit size has been reduced, the relative stopband width has worsened. In order to maximize stopband properties, it is preferable to employ an appropriate cascaded irregular shape resonator [15] with variable attenuation frequencies. Improving roll-off and stopband properties, on the other hand, is challenging.

Received 25 February 2022, Accepted 24 March 2022, Scheduled 5 April 2022

* Corresponding author: Thevaruparambil Abdulnazer Nisamol (nisamolshiyas2018@cusat.ac.in).

[1] Division of Electronics, School of Engineering, Cochin University of Science and Technology, 682022, India. [2] Department of Electronics, N S S College Rajakumari, 685619, India.

The transmission and stub line modification approach results in better performance and NCS features. This paper features a high RSB of 185.4% with 20 dB suppression up to 40 GHz and low NCS $0.10\lambda_g^2$ by using the poly-resonators associated with the proposed inclined stepped impedance transmission line (ISTL) filter. The novel approach of chamfering in the stepped impedance section along with the resonator modules creates a filter with the rejection up to 26th order harmonics. This unique technique of using 120° inclination is provided with chamfering at the bend discontinuity which reduces the radiation loss. The method is well applicable to the existing straight transmission line structures having NCS issues and can be successfully implemented at the demodulation section in the receiver side of the communication systems.

2. DESIGN OF INCLINED STEPPED IMPEDANCE TRANSMISSION LINE (ISTL) FILTER

The inclined transmission line with the central stepped model employed in the proposed structure has a major contribution in compressing the circuit size of the filter. It is designed with the central angle 'θ' = 120° and can be observed from Figure 1(a). The central angle of ISTL is the same as the radial angle of the radial stub resonator (RSR). The angle optimization of ISTL is carried out using RSR with transmission zero occurring at 4.1 GHz. The return loss and insertion loss of the filter are strictly affected by the value of 'θ'. The discontinuity arises at the central angle which creates degeneration of higher-order harmonics in the stopband frequencies. It is an abrupt geometrical deviation of the transmission line, and a stepped impedance is provided at the center of the inclined transmission line to avoid excess charge accumulation. It is effective to use chamfering [16] at this patch corner as shown in Figure 1(b) to reduce the extra fringing field at the outer section of the ISTL.

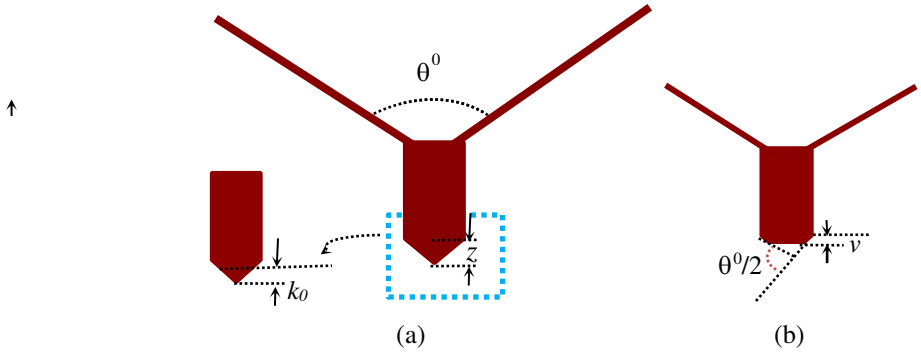

Figure 1. Inclined stepped impedance transmission line with unchamfered and chamfered end. (a) Unchamfered ISTL. (b) Chamfered ISTL.

Figures 2(a)–(b) show transmission characteristics of the chamfered ISTL compared with the unchamfered ISTL. The deviation of attenuation level of 16 dB from the unchamfered ISTL is also observed. The percentage chamfering (%C) can be calculated from Eq. (1).

$$\%C = \left[1 - \frac{y}{z}\cos\left(\frac{\theta}{2}\right)\right] \times 100\% \tag{1}$$

Equation (1) will be satisfied when the remaining width 'y' after chamfering is half of the $z = 2k_0$, where k_0 is the chamfered cut-out portion. The discontinuity configuration is optimized with percentage chamfering to attain minimum reflection coefficient and radiation loss. This creates a significant attenuation rate for chamfered ISTL compared to a sharp edge. The %C, insertion loss (IL), passband return loss (RL), and cut-off frequency variation with the central angle is plotted in Figure 3. The passband return loss surge is noticed with 'θ'; however, it is optimized after considering the reduction in insertion loss. Furthermore, the stopband IL is augmented with a central angle, and the overall 75% chamfering is optimized with 120° inclination. Beyond this inclination, the geometrical compactness will be affected. To minimize excess fringing field, the chamfered outer corner is attached with a central

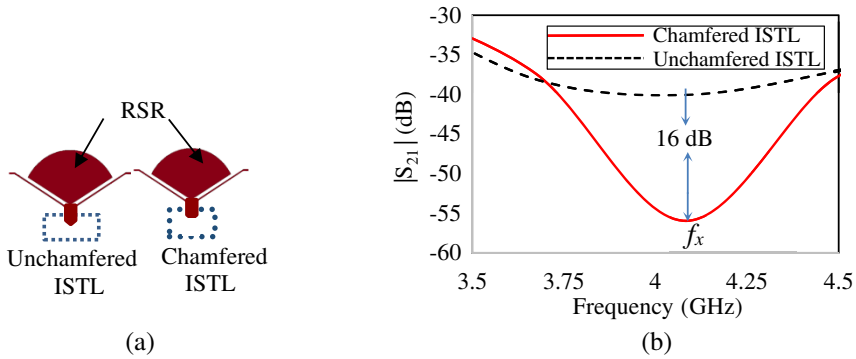

Figure 2. Comparison of conventional transmission line filter with unchamfered ISTL and proposed ISTL filter with RSR. (a) Structural diagram. (b) S_{21} comparison between chamfered and unchamfered ISTL.

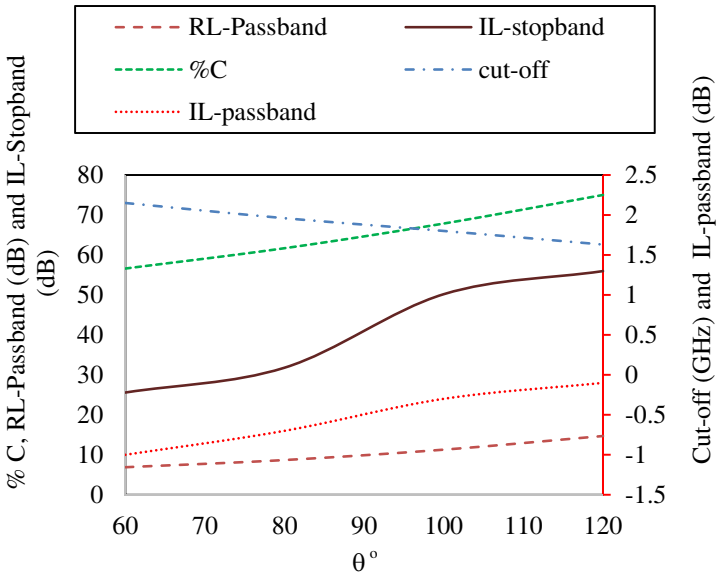

Figure 3. Central angle optimization of ISTL and RSR (RL-return loss, IL-Insertion loss).

low impedance section (CLI), and this will reduce the radiation loss created due to 120° bend. The CLI improves the capacitive impedance even though it consists of vertical leads downwards.

The conventional transmission line (CTL) and ISTL with CLI sections shown in Figure 4(a) are compared analytically, and Equations (2) and (3) are derived for the first transmission zeros. The coupling capacitance $C_c = 0.03\,\text{pF}$ in Figure 4(b) imparts the ISTL coupling with RSR, and it is noticed that CTL has the transmission zero shift from the cut-off frequency compared to ISTL in Figure 5. A frequency shift of 16% is observed with a 1.51 GHz cut-off frequency. The deviation in suppression level noticed in the EM simulation results is due to the material losses which are not considered in LC simulation. The capacitive impedance of CLI provides higher significance in the suppression of lower frequency transmission zeros in the stopband region.

$$f_0 = \frac{1}{2\pi\sqrt{L_2C_2}} = 3.83\,\text{GHz} \tag{2}$$

$$f_1 = \frac{1}{2\pi}\sqrt{\frac{C_1 + 2C_2}{C_1C_2L_1 + C_C(L_1 + L_2)(C_1 + 2C_2)}} = 3.26\,\text{GHz} \tag{3}$$

The transmission zero of RSR on ISTL ($f_x = 4.1\,\text{GHz}$)) shifts to f_1 in Figure 5 owing to the impact

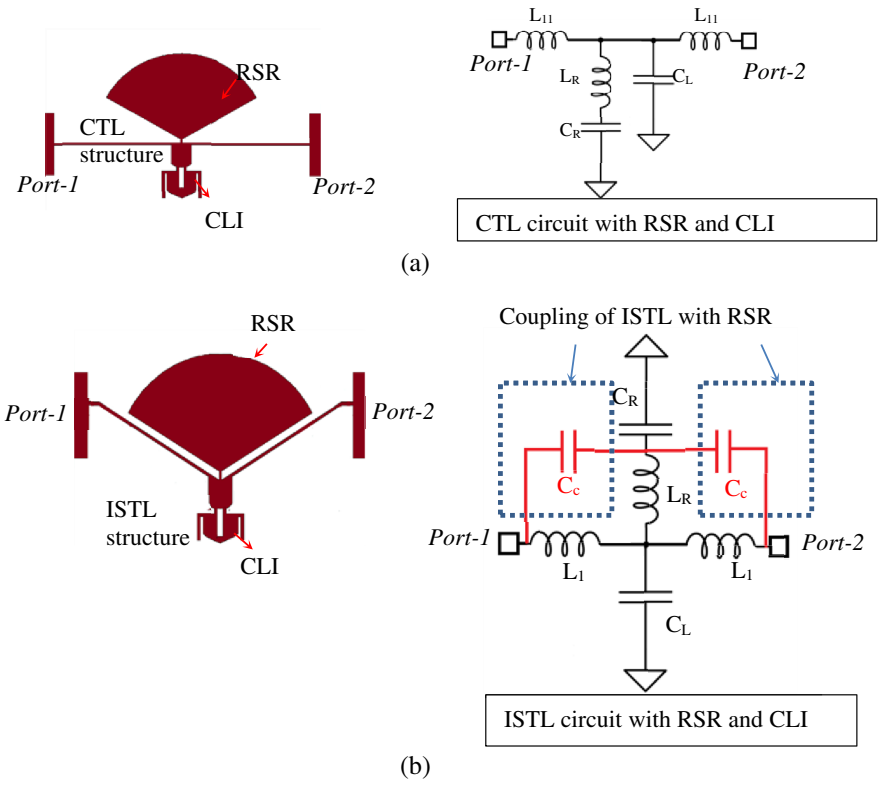

Figure 4. Comparison between conventional and inclined transmission line. (a) CTL and ISTL simulated structure. (b) Equivalent LC circuits with values $L_{11} = 9.332\,\text{nH}$, $L_1 = 5.5\,\text{nH}$, $L_R = 0.75\,\text{nH}$, $C_L = 0.9\,\text{pF}$, $C_R = 2.3\,\text{pF}$, $C_c = 0.035\,\text{pF}$.

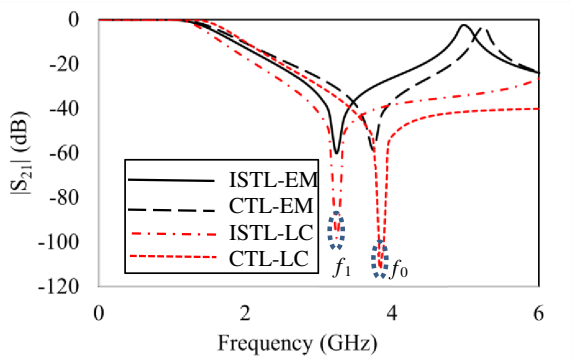

Figure 5. EM and LC comparison chart between conventional and inclined transmission lines.

of CLI. The equivalent circuit of the ISTL and the formula for the transmission zero 'f_0' is derived in Eq. (2). 'f_0' is a function of the lumped element values L_2 and C_2 of RSR based on Eq. (2).

The shifted frequency f_1 is derived in Eq. (3) using the ISTL equivalent circuit by considering the coupled capacitance, C_c. Figure 6(a) points out the variation of f_1 with respect to the lumped impedance values of RSR (C_2 and L_2) and C_c. As per the derived equation, f_1 is found to be inversely proportional to the impedance values. A small fluctuation in f_1 with respect to C_1 is also noted for the ISTL structure due to the change in the circuit combination of LC values. Figure 6(b) shows the cut-off frequency deviation, and CLI (C_1) contributes major shift.

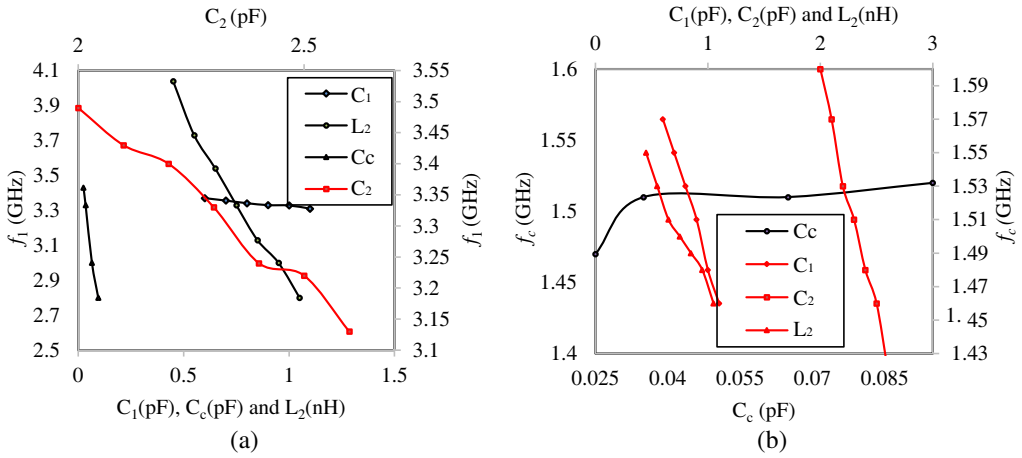

Figure 6. Parametric effects of RSR and CLI. (a) For controllable Transmission zero (f_1). (b) For controllable cut-off frequency.

3. RESONATOR MODULES (RM)

The noise rejection beyond 20 GHz is made possible by using resonator modules (RM). They are placed on the ISTL symmetrically on both sides of the input and output ports.

3.1. Resonator Module-1 (RM_1)

The inclined high impedance stub of RM_1 components provides higher roll-off characteristics and high-frequency transmission zeros to the final frequency response. It is essential to create a number of attenuation peaks (beyond 20 GHz) for the extended range of frequency rejection bands. The RM_1 components A_1, A_2, and A_3 are shown in Figures 7(a)–(c) with inclination angle θ_1, θ_2, and θ_3, respectively. The resonator module A_1 has the inclination at the high impedance stub, and A_2 has inclination at the low impedance patch. The small change in the inclination angle affects the spacing between the resonators and thereby compactness of the filter. The parallel inclination created at stub and patch sections of A_3 increases the coupling environment with the transmission line and decreases the circuit size of the overall filter.

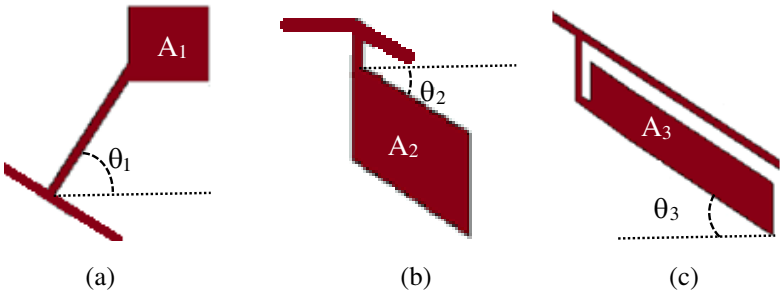

Figure 7. RM_1 components (a) A_1 with $\theta_1 = 60°$. (b) A_2 with $\theta_2 = 45°$. (c) A_3 with $\theta_3 = 45°$.

The gradual formation of transmission zeros at higher frequencies in the particular intervals makes the stopband extended up to 40 GHz. Furthermore, the RM_1 sections A_1, A_2, and A_3 show a significant change in the cut-off frequency of the filter as shown in Figure 8(a).

The multiple low-frequency transmission zeros are formed at each interval of frequencies T_{L1}, T_{L2}, T_{L3}, and T_{L4}, which can be observed in Figure 8(b). The intervals possess different attenuation levels, and the addition of each RM_1 component increases the overall attenuation levels and promotes more high frequency signal isolation.

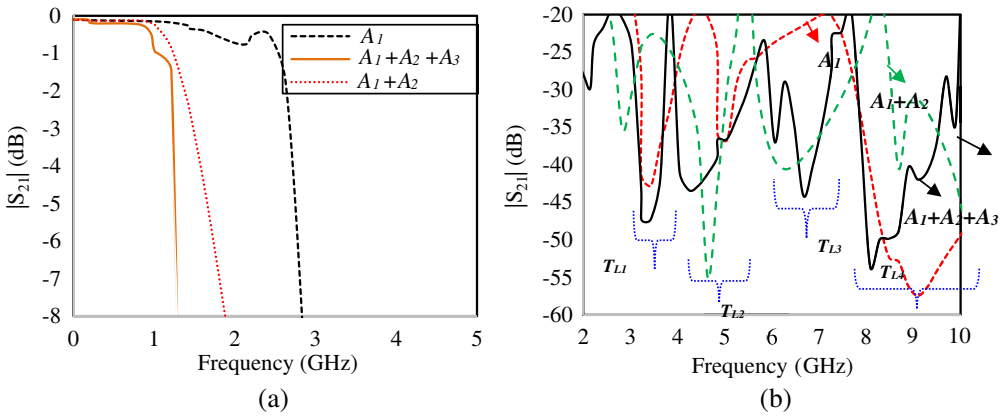

Figure 8. Analysis of RM_1 components. (a) Cut-off frequency deviation on adding RM_1 sections. (b) Formation of low-frequency transmission zeros.

3.2. Resonator Module-2 (RM_2)

RM_2 is a combination of the triangular resonator (TR), open stub (OS), and semicircular resonator (SR) shown in Figure 9(a). The LC equivalent circuit for the RM_2 network is shown in Figure 9(b). The bend compensated impedance also plays a significant role in the stopband characteristics. These resonators create a coupling environment in the poly-resonator ISTL filter and increase the suppression of higher-order harmonics. The more coupling effect of ISTL than conventional transmission line provides deeper transition characteristics from passband to stopband since the TR in RM_2 imparts the transmission zero at 1.94 GHz with a deep suppression as observed from Figures 10(a)–(b). The capacitive OS provides additional suppression to the stopband frequencies.

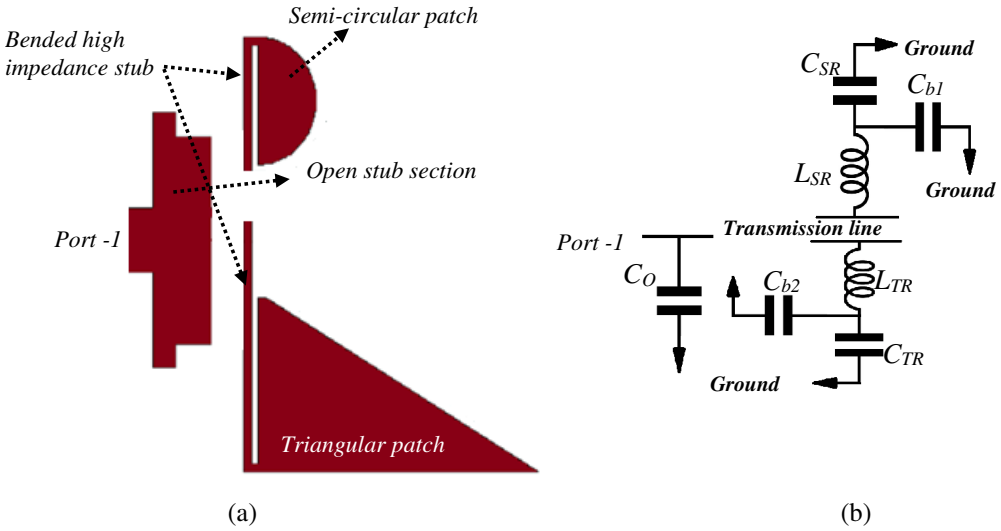

Figure 9. RM_2 components. (a) Planar model. (b) LC model with $C_{SR} = 0.324$ pF, $C_{TR} = 1.604$ pF, $L_{SR} = 3.4985$ nH, $L_{TR} = 6.4782$ nH, $C_{b1} = C_{b1} = 0.06$ pF, $C_O = 0.585$ pF.

The RM_2 sections have less significant effects on cut-off frequencies as they are mostly used as suppressing cells. Equations (4) and (5) are derived from the transfer function analysis of the irregularly shaped stubs and patches of the RM_2. The effect of bend compensated capacitor C_{b1} and C_{b2} corresponds to the 90°-bend angle at the high impedance stubs of SR and TR which have significance in the position

of transmission zeros.

$$f_{SR} = \frac{1}{2\pi\sqrt{L_{SR}(C_{SR} + C_{b1})}} \tag{4}$$

$$f_{TR} = \frac{1}{2\pi\sqrt{L_{TR}(C_{TR} + C_{b2})}} \tag{5}$$

Open stubs are utilized to extract leftover signals at the output of SR and TR and thereby enhance the suppression behavior of the final frequency characteristics. The RM_1 and RM_2 components in Figure 10(a) are designed with lumped element inductors and capacitors, and the resonance of each module is calculated for the wide stopband extension. They are symmetrically arranged on both sides of the central RSR or the sides of port-1 and port-2. The symmetrical coupling increases the effective impedance of the circuit and enhances the capability to extract the undesired frequencies up to 40 GHz with higher suppression.

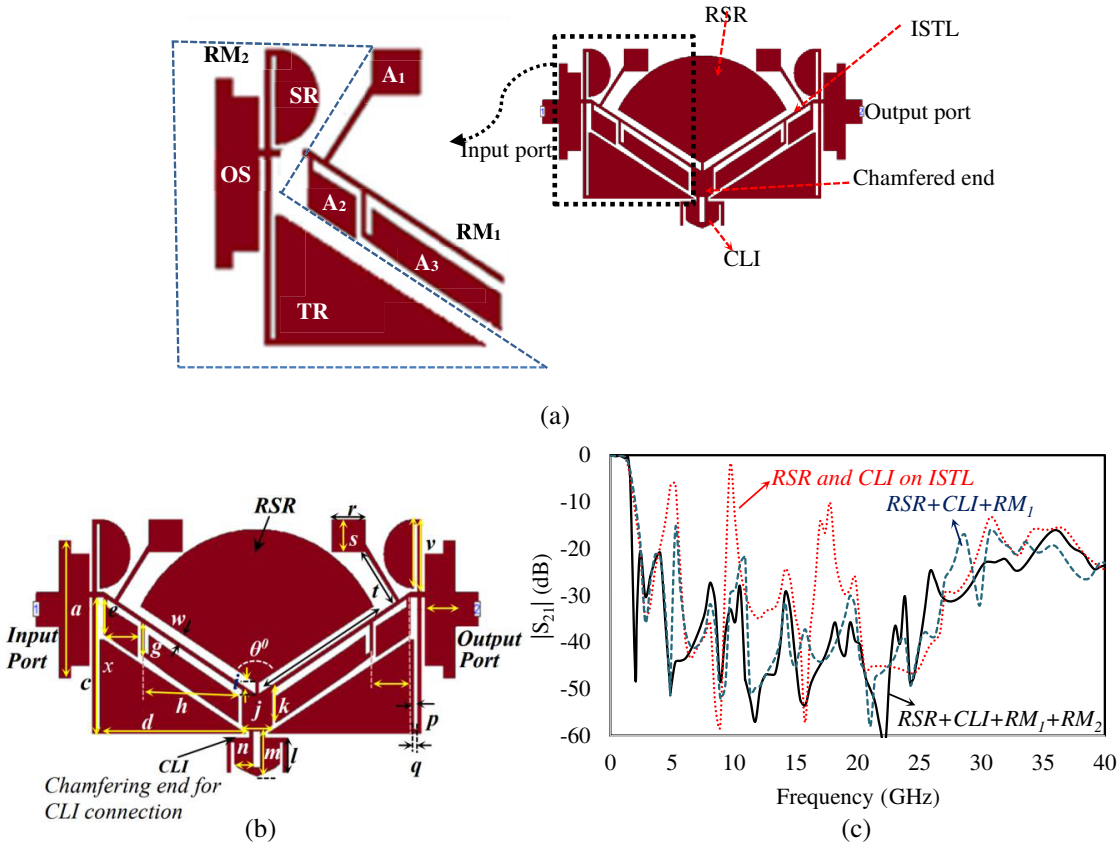

Figure 10. Significance of RM_1 and RM_2. (a) RM_1 and RM_2 modules symmetrically on both sides of the port. (b) Proposed layout of Poly-resonator Poly-resonator ISTL filter $a = 7.3$, $b = 2$, $c = 8.04$, $d = 9.8$, $e = 1.7$, $f = 2.25$, $g = 1.95$, $h = 6.2$, $i = 0.7$, $j = 1.4$, $k = 2.4$, $l = 2.75$, $m = 2.65$, $n = 1.5$, $o = 2.65$, $p = 0.2$, $q = 0.2$, $r = 2.3$, $s = 1.85$, $t = 4.1$, $u = 4.05$, $v = 4.25$, $w = 0.55$, $x = 11.87$. (All measurements are in mm). (c) Section-wise frequency characteristics showing prolonged improvements in RSB.

Table 1 shows the designed and practical resonance frequencies for each resonator component up to 25 GHz. The frequency at which the transmission zero occurs is highly significant in the design of a filter. Resonator modules are designed for the specific transmission zeros at higher frequencies beyond the cut-off frequency. The practical LC simulation results obtained using the designed lumped elements are also calculated in the table. Further stopband extension up to 40 GHz is due to the occurrence of multiple resonance created by each module at each stopband frequency interval of the proposed

Table 1. Transmission zero analysis using equation and EM simulation of each resonator modules.

Resonator Modules (y)	Design $f_y = \frac{1}{2\pi\sqrt{LC}}$ (GHz)			Practical results (EM simulation) f (GHz)
	L_y (nH)	C_y (pF)	f_y (GHz)	
A_1	3.144	0.167	6.9	6.5
A_2	0.393	0.1033	24.9	24.6
A_3	1.533	0.9325	4.2	3.22
SR	3.4985	0.324	4.727	5
TR	6.4782	1.604	1.5613	2.02

response. Lowpass filter at the receiver section can be used to extract low frequency message signals at lower Gigahertz range from the modulated signal. The proposed circuit blocks the higher harmonics carrier signals and noise interruption up to 40 GHz.

The lumped element values for each component are calculated with effective dielectric constant $\varepsilon_{eff} = 1.92$. Open stubs having capacitance C_0 are also selected for the further rejection of the higher harmonics. The developed equivalent circuit is shown in Figure 11(a). The circuit consists of two 'T' networks (P_1), two 'π' networks (P_2), and two parallel networks (P_3) along with the CLI and RSR components. The dual combinations of P_1, P_2, and P_3 are introduced to suppress maximum signals propagated through the ISTL beyond cut-off frequency. The frequency characteristics associated with the proposed equivalent circuit are compared with the EM model, and it is illustrated in Figure 11(b). The coupling capacitance C_c is considered to make it practical and have better analogous lumped element results with less tolerance error.

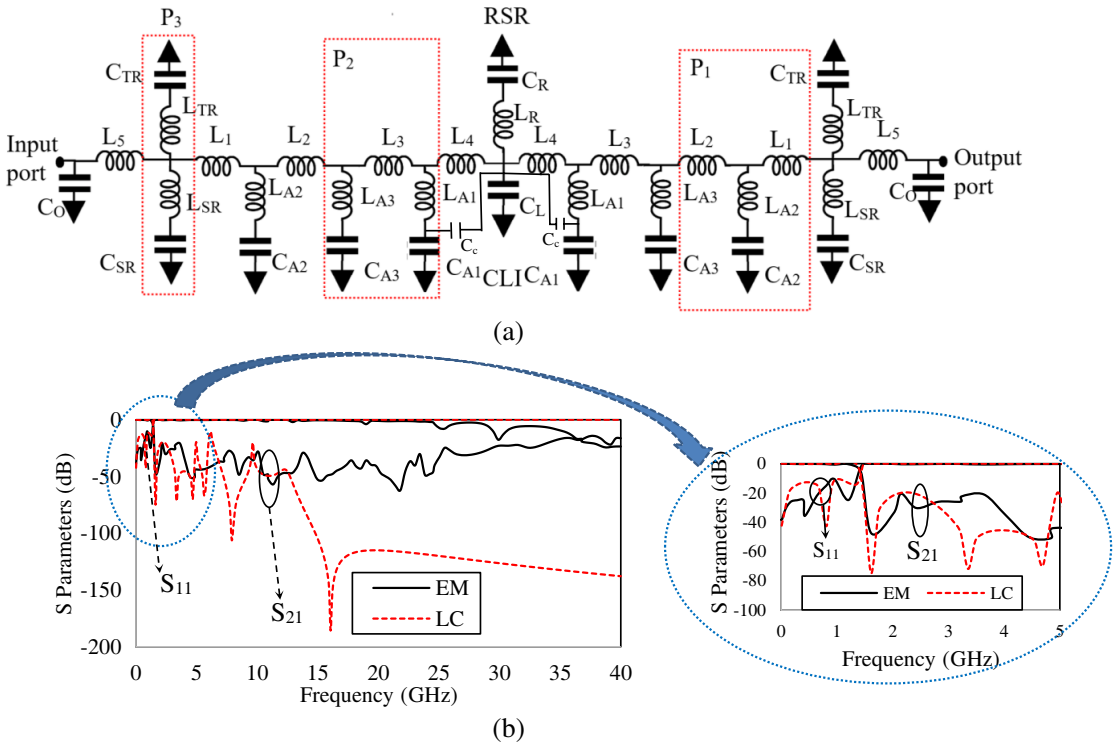

Figure 11. The equivalent circuit developed for the final cascaded structure. (b) The EM and LC simulation results comparison.

The occurrence of bend impedances is compensated effectively by the main inductances and capacitance of the resonator sections. The other values are $L_1 = L_2 = 0.393\,\text{nH}$, $L_3 = 0.982\,\text{nH}$, $L_4 = 5.346\,\text{nH}$, and $L_5 = 0.157\,\text{nH}$.

The final transmission characteristics with the wideband response up to 40 GHz are displayed in Figures 12(a)–(b). The rejection level of 20 dB is observed with the broadband characteristics. The flat group delay at the passband is illustrated in Figure 12(c), and it is significant to achieve flat and consistent group delay over the passband frequencies which is vastly relevant in monopulse receivers to achieve null depths. The message signals up to 1.51 GHz will propagate through the transmission line as seen from the electric field distribution shown in Figures 13(a)–(b). The information within the signals is reliably retrieved at the output.

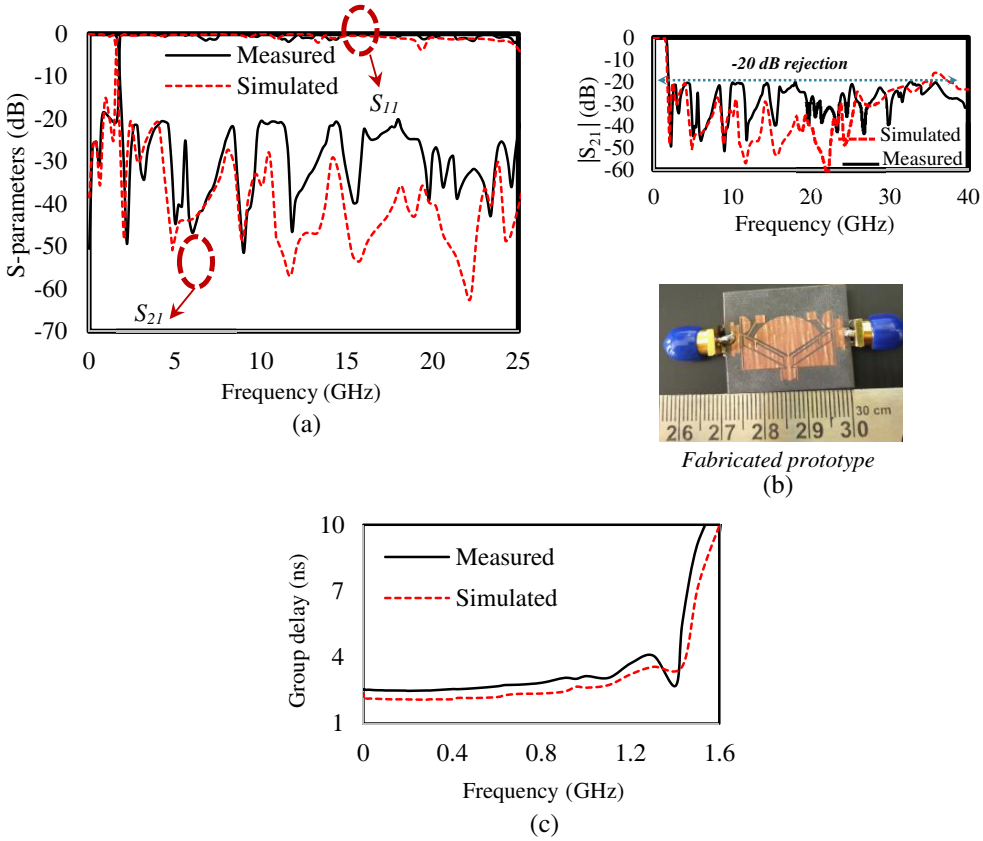

Figure 12. Experimental verifications. (a) S Parameter. (b) Wide stopband S_{21} response. (c) Group delay.

The carrier signals are blocked at the TR and SR which is observed in Figures 13(c)–(d).

The further rejection of higher harmonics and noise interruptions are achieved due to the combined effects of low impedance RSR and CLI. The highest attenuation of the EM signals at the output port is achieved based on the number of fields accumulated on the poly-resonators without radiation loss. The suppression factor (SF) of 2 with 163 dB/GHz roll-off rate (ROR) is achieved using the RT/Duroid 5880 substrate with 2.2 permittivity and 0.79 mm thickness. Simulation and optimization of the structure were conducted in the IE3D platform. The performance evaluation of this letter with the latest works of literature in terms of RSB, NCS, SF are compared in Table 2, and comparatively high RSB and low NCS are accomplished for the proposed structure. The wide frequency rejection band up to 40 GHz is achieved with 26th order harmonic suppression which is superior to the existing literatures.

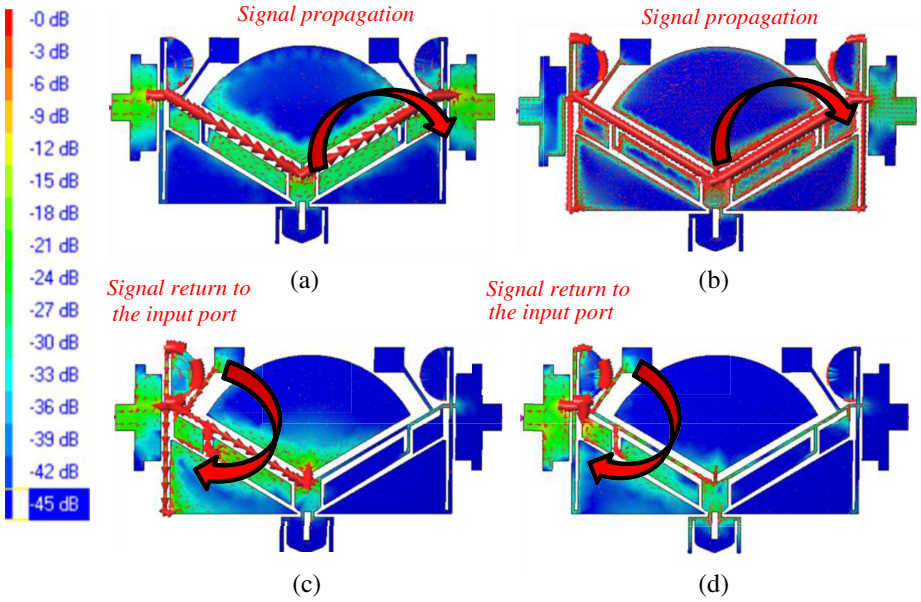

Figure 13. The Electric Field distribution. (a) At 0.1 GHz. (b) At 1 GHz. (c) At 5 GHz. (d) At 20 GHz.

Table 2. Verification of performance advancement compared with existing literature.

Ref	f_c (GHz)	SF	RSB	NCS ($\times\lambda_g^2$)	ROR	Technique used
[1]	2.68	2	1.51	0.024	308.3	Resonators and stubs
[2]	3	2	1.06	0.74	34	Defective ground model
[3]	1.4	2.3	0.65	2.7	47.4	Metamaterial
[4]	2.44	2.2	1.39	0.038	67.27	Patch and stub resonators
[5]	0.72	2	1.67	0.0378	ng	Square ring loaded resonators
[6]	1.26	2	1.65	0.035	217	Circular patches and open stubs
[11]	2.078	2.2	1.45	0.0176	118.6	Cascaded modified patch resonators
[14]	2.11	1.8	1.59	0.032	100	Defected ground and Spur line resonator
[15]	1.27	2.5	1.76	0.048	92.5	Cascaded pentagonal resonator
This letter	1.51	2	1.85	0.010	163	Chamfered ISTL and poly-resonators

*ng: not given

4. CONCLUSION

The inclined stepped impedance transmission line and poly-resonators compress the NCS of the filter and also enhance the coupling between the transmission line and resonators. The novel approach of chamfering provided in the stepped discontinuity of ISTL diminishes the radiation losses and improves the suppression level. The relative stopband width of 185.4% with 26th harmonic suppression is obtained from the presented poly-resonator ISTL filter utilizing RM_1 and RM_2 resonator modules. NCS is reduced to 16.6% with inclined lines compared to the conventional transmission lines with additional stopband behaviour. The presented structure is appropriate for passing the existing L band message signals in the demodulator section of the communication applications having simultaneous issues in NCS and RSB.

REFERENCES

1. Moloudian, G., S. Bahrami, and R. M. Hashmi, "A microstrip lowpass filter with wide tuning range and sharp roll-off response," *IEEE Transactions on Circuits and Systems II: Express Briefs*, Vol. 67, No. 12, 2953–2957, 2020.
2. Boutejdar, A., M. Challal, and S. El Hani, "Design of a new broad stop band (BSB) lowpass filter using compensated capacitor and II-H-II DGS resonator for radar applications," *Progress In Electromagnetics Research M*, Vol. 73, 91–100, 2018.
3. Paul, B. J., S. Mridula, B. Paul, and P. Mohanan, "Metamaterial inspired CPW fed compact low-pass filter," *Progress In Electromagnetics Research C*, Vol. 57, 173–180, 2015.
4. Rekha, T., P. Abdulla, P. M. Raphika, and P. M. Jasmine, "Compact microstrip lowpass filter with ultra-wide stopband using patch resonators and open stubs," *Progress In Electromagnetics Research C*, Vol. 72, 15–28, 2017.
5. Li, Z. and S. J. Ho, "Compact microstrip lowpass filter with ultra-wide stopband characteristic using square ring loaded resonators," *Progress In Electromagnetics Research Letters*, Vol. 90, 1–5, 2020.
6. Karimi, G., A. Lalbakhsh, and H. Siahkamari, "Design of sharp roll-off lowpass filter with ultra-wide stopband," *IEEE Microwave and Wireless Components Letters*, Vol. 23, No. 6, 303–305, 2013.
7. Nouri, L., S. Yahya, and A. Rezaei, "Design and fabrication of a low-loss microstrip lowpass-bandpass diplexer for WiMAX applications," *China Communications*, Vol. 17, No. 6, 109–120, 2020.
8. Deng, P. H., J. T. Tsai, and R. C. Liu, "Design of a switchable microstrip dual-band lowpass-bandpass filter," *IEEE Microwave and Wireless Components Letters*, Vol. 24, No. 9, 599–601, 2014.
9. Choudhary, D. K. and R. K. Chaudhary, "Compact lowpass and dual-band bandpass filter with controllable transmission zero/center frequencies/passband bandwidth," *IEEE Transactions on Circuits and Systems II: Express Briefs*, Vol. 67, No. 6, 1044–1048, 2019.
10. Chau, W. M., K. W. Hsu, and W. H. Tu, "Filter-based Wilkinson power divider," *IEEE Microwave and Wireless Components Letters*, Vol. 24, No. 4, 239–241, 2014.
11. Jamshidi, M. B., A. Lalbakhsh, B. Mohamadzade, H. Siahkamari, and S. M. H. Mousavi, "A novel neural-based approach for design of microstrip filters," *AEU — International Journal of Electronics and Communications*, Vol. 110, 152847, 2019.
12. Fan, M., K. Song, and Y. Fan, "Reconfigurable low-pass filter with sharp roll-off and wide tuning range," *IEEE Microwave and Wireless Components Letters*, Vol. 30, No. 7, 649–652, 2020.
13. Xiao, M., G. Sun, and X. Li, "A lowpass filter with compact size and sharp roll-off," *IEEE Microwave and Wireless Components Letters*, Vol. 25, No. 12, 790–792, 2015.
14. Rekha, T. K., P. Abdulla, P. M. Jasmine, and A. R. Anu, "Compact microstrip lowpass filter with high harmonics suppression using defected structures," *AEU — International Journal of Electronics and Communications*, Vol. 115, 153032, 2020.
15. Lalbakhsh, A., M. B. Jamshidi, H. Siahkamari, A. Ghaderi, A. Golestanifar, R. Linhart, J. Talla, R. B. Simorangkir, and K. Mandal, "A compact lowpass filter for satellite communication systems based on transfer function analysis," *AEU — International Journal of Electronics and Communications*, Vol. 124, 153318, 2020.
16. Maramis, H. J. and K. C. Gupta, "Planar analysis and optimization of microstrip discontinuities," 1988.